PROCEDURE OF EXTRACTING THIN ICE AREAS IN THE SEA OF OKHOTSK USING MODIS DATA

K. Cho [1]*, K. Naoki [1]

[1]Tokai University Research & Information Center , 2-3-23, Takanawa, Minato-ku, Tokyo, 108-8619, Japan, kohei.cho@tokai-u.jp

Commission III

KEY WORDS: sea ice, Aqua, global warming, ice thickness, RSI, OLI

ABSTRACT:

The latest IPCC report clearly stated that the human influence is the main reason of sea ice reduction in the Arctic. Importance of sea ice monitoring from space is increasing. In addition, the heat flux of ice in thin ice areas is strongly affected by the ice thickness difference. Therefore, ice thickness is one of the important parameters of sea ice. The authors have been studying on extracting thin ice areas using optical sensor such as MODIS for years. In this paper, the authors summarized the procedure of our study starting from comparing in-situ measurement of ice thickness with high resolution optical sensor RSI data, and finally developing the thin ice area extraction algorithm using MODIS. Estimating ice thickness from optical sensor data is not easy. However, through our study, the authors have verified the possibility of extracting thin ice areas using optical sensor data observed from satellites. In this study, the authors define “thin ice areas” as ice which thickness is less than about 30cm with reflectance much lower than thick ice. The basic idea of the algorithm is to use the scatterplots of MODIS band 1 & 2 reflectance and extract thin ice areas using the distribution difference of thin ice against water, thick ice, clouds. Not all but most of the thin ice areas could be extracted using the algorithm.

1. INTRODUCTION

The sixth Assessment Report of IPCC (2021) says that human influence is very likely the main driver of the decrease in the Arctic Sea ice area between 1979–1988 and 2010–2019 (decreases of about 40% in September and about 10% in March). The importance of sea ice monitoring from space is increasing. Under the cloud free condition, optical sensors onboard satellites allow us to monitor the detailed condition and distribution of sea ice with wide view. In monitoring sea ice, ice thickness is one of the important parameters. Various studies on estimating ice thickness with optical sensors onboard satellites have been performed in the past including Allison (1993), Perovich et al. (1982), Grenfell (1983), Mäkynen (2017). Basically, the reflectance of ice increases as the ice thickness increases. However, since the reflectance of sea ice is likely to be affected by the freezing condition and snow cover, the relationship between ice thickness and its reflectance (albedo) varies between different observations (See Figure 1). Also, the reflectance of ice would be saturated at certain thickness and snow cover. These results suggest the difficulty of estimating sea ice thickness from optical sensor observation from space. However, since the reflectance of thin ice is much lower than that of thick ice, the extraction of thin ice area from optical sensor data should be possible. Since the heat flux of ice is strongly affected by the ice thickness (Maykut, 1978), extracting thin ice area is quite important. Thus, author has been studying the possibility of extracting thin ice areas using optical sensor such as MODIS on Terra and Aqua satellites.

In this paper, the authors summarize the procedure of our study starting from comparing in-situ measurement of ice thickness with high resolution optical sensor RSI data, and finally developing the thin ice area extraction algorithm using MODIS. The definition of “thin ice areas” in this study is the ice areas which thickness is less than about 30cm which reflectance is lower than thick ice.

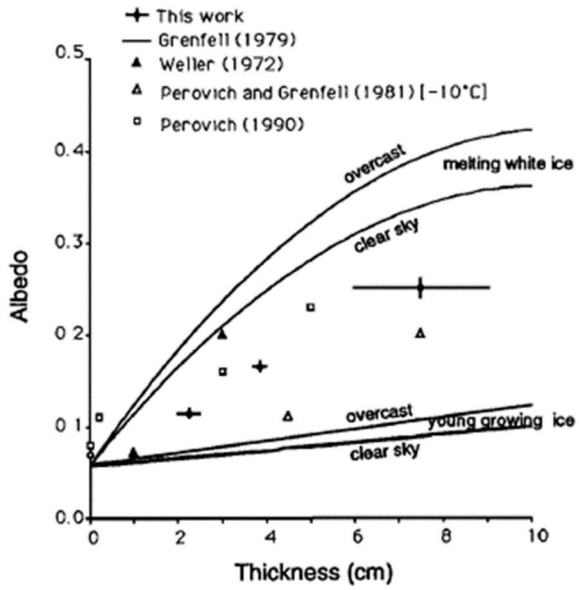

Figure 1. Relationship between ice thickness and albedo. (Allison, 1993)

2. 2. TEST SITE

The authors have selected the Sea of Okhotsk as the test sites in this study. As for the in-situ measurement, Monbetsu Bay and Saroma Lake located along the coast of Hokkaido, Japan were selected as test sites. Figure 2 show the map of the test sites. The Sea of Okhotsk is located at the north side of Hokkaido, Japan, surrounded by the Island of Sakhalin and eastern Siberian coast**,** Kamchatka Peninsula and Kuril Islands. The sea is one of the most southern seasonal sea ice zones in the northern hemisphere, and many thin ice areas can be found in the sea.

*Corresponding author: Kohei Cho, Tokai University Research & Information Center, Takanawa, Minato-ku, Tokyo, 108-8619, Japan

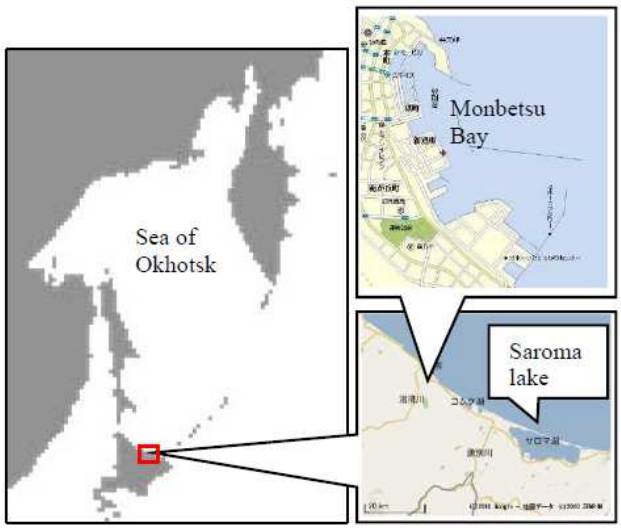

Figure 2. Map of the test sites.

3. ANALYZED DATA

The optical sensor data from RSI onboard FOROMSAT-2 satellite, OLI onboard Landsat-8 satellite and MODIS onboard Aqua satellite were used in this study. Table 1 show the specifications of the three sensors. In order to utilize the highest spatial resolution of MODIS, only Band 1 and 2 which have 250m resolution were used for the analysis. However, 250m spatial resolution is still too low for comparing with the in-situ measurement. So, RSI data with the spatial resolution of 8m was used for comparing the radiance measured from space with the in-situ measurement data of ice thickness. In order the evaluate the thin ice areas extracted from MODIS data, the optical sensor OLI images of Landsat-8 were used as references. The spectral bands similar to MODIS band 1 and 2 were selected from RSI and OLI bands respectively.

Table 1. Specifications of optical sensors

Sensor	Band	Wavelength	IFOV	Swath
RSI	3	0.63 - 0.69μm	8m	24km
	4	0.76 - 0.90μm		
OLI	4	0.64 - 0.68μm	30m	185km
	5	0.85 - 0.88μm		
MODIS	1	0.62 - 0.67μm	250m	2330km
	2	0.84 - 0.88μm		

MODIS(2010), RSI(2011), OLI(2014)

4. METHODOLOGY

4.1 Comparison of Ice Thickness and Reflectance based on In-situ Measurement

In-situ measurement of ice reflectance and thickness were performed at Monbetsu Bay and Saroma Lake of Hokkaido, Japan. The ASD FieldSpec HandHeld spectrometer (2006) was used for measuring the ice reflectance. The ice thickness measurement was performed by using a drill and a measure. A small vessel was used for the measurement. Figure 3 show the snap shots of the measurement. Figure 4 show the sample points of ice reflectance and ice thickness measurement plotted on an aerial photo of a part of Monbetsu bay taken on February 22, 2007. Figure 5 shows the relationship between ice thickness and reflectance. It is clear that if the measurement is performed at a thin ice (which thicknesses were less than 15cm) area where the sea ice froze in same condition with less snow cover, ice thickness and reflectance show a proportional relationship. However, since the reflectance of sea ice is likely to be affected by the freezing condition and snow cover, the relationship between ice thickness and reflectance starts to scatter with the enlargement of observation areas. Figure 6 shows such an example which measurements were performed in wider sea ice areas. These results suggested the possibility and limitation of identifying ice thickness differences from ice reflectance. Also, we have to recognize that the reflectance of satellite data is the averaged reflectance of various types of ice and water in one pixel size.

(a)Reflectance measurement (b)Ice thickness measurement

Figure 3. In-situ measurement from a vessel.

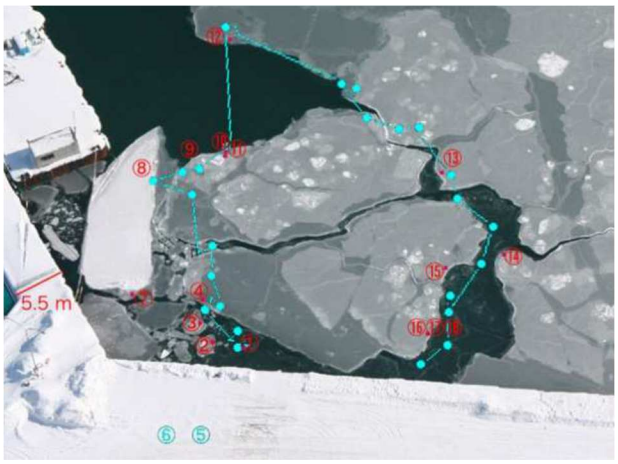

Figure 4. Sample points of ice reflectance and ice thickness measurement. (Monbetsu Bay, February 22, 2007).

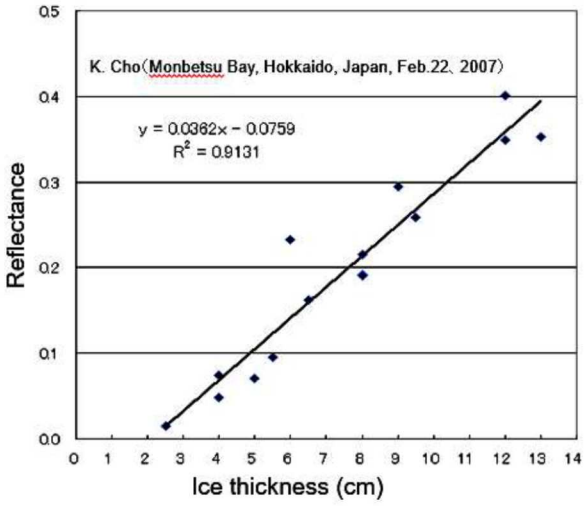

Figure 5. Relationship between ice thickness and reflectance (Monbetsu Bay, February 22, 2007)

This contribution has been peer-reviewed. The double-blind peer-review was conducted on the basis of the full paper.
https://doi.org/10.5194/isprs-annals-V-3-2022-319-2022 | © Author(s) 2022. CC BY 4.0 License.

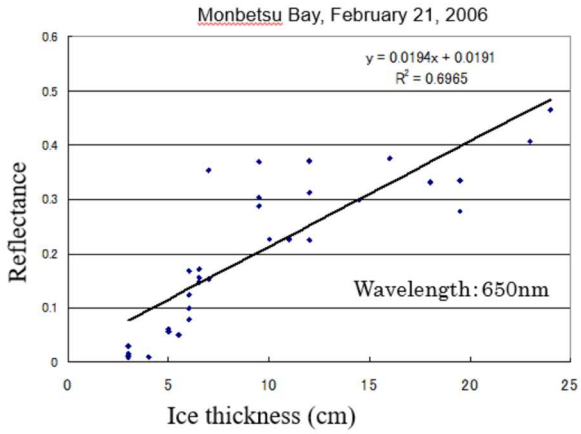

Figure 6. Relationship between ice thickness and reflectance (Monbetsu Bay, February 21, 2006)

4.2 Comparison of Ice Thickness and RSI Radiance

In order to evaluate the possibility of estimating thin ice thickness with optical sensors on board satellites, direct measurements of ice thickness were performed in Saroma Lake and Monbetsu Bay in February 2011 and 2012 (Cho et. Al., 2011, 2012). Figure 7 show sample points plotted on the RSI images. Figure 8 show the relationship between the ice thickness and the radiance derived from RSI band 3 and 4 data measured at the points shown in Figure 7. Since thin ice areas are likely to be wet, the radiance of band 3 (visible) were rather higher than band 4 (near IR). However, basically, the proportional relationship was observed between the ice thickness and the radiance acquired by RSI for the thin ice area around the mouth of the lake when the ice thicknesses were less than 20cm. This result suggests the possibility of estimating ice thickness of thin ice with high resolution optical sensor such as RSI under the snowless and cloud free condition. Since the data were taken in two different places with one year interval, the result also suggested the stability and reliability of RSI data. As for the ice thicker than 20cm, our previous study (Cho et. al., 2011) suggested the difficulty of estimating ice thickness from reflectance mainly due to the snow cover on the ice.

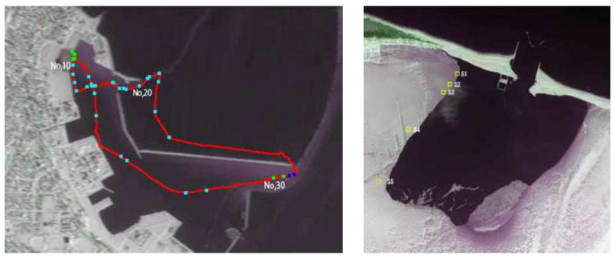

(a) Monbetsu Bay (Feb. 26, 2011) (b) Saroma Lake (Feb. 25, 2012)

Figure 7. Measured points plotted on RSI images

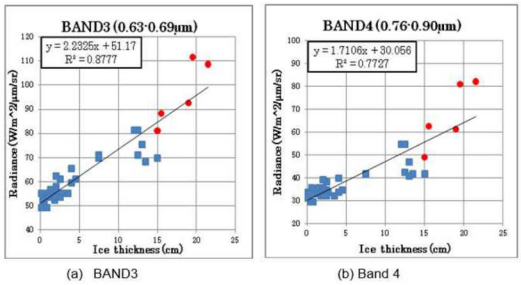

(a) BAND3 (b) Band 4

Figure8. Relationship between ice thickness and RSI radiance.

4.3 Comparison of RSI Radiance and MODIS Radiance

In the next step, the RSI radiance and MODIS radiance observed on the same day over the Saroma Lake were compared. The RSI and MODIS images analysed in this study are shown on the Figure 9. Saroma Lake is a brackish lake connected to the Sea of Okhotsk by the two mouths. In the images of Figure 9, open water area can be seen near the one of the mouths, and dark purple area in the center of the lake. In these RGB composite images, red band (RSI band 3 and MODIS band 1) is assigned to R and B, and near IR band (RSI band 4 and MODIS band 2) is assigned to G. In thin ice areas, the reflectance of both bands become low. Moreover, the surface of thin ice is likely to be wet. As a result, reflectance of near IR band becomes much lower than that of red band and appears in dark purple in these color composite images. The radiance of RSI and MODIS of the box area in Figure 9 were compared. Figure 10 shows the scatter plots of RSI radiance versus MODIS radiance for visible and near IR bands. Due to the scheduling constraint, the authors could not measure the ice thickness of the area on this day. However, by comparing Figure 8 and 10, it may be fair to say that thin ice areas with less than around 30cm could be identified as dark purple areas in the MODIS images.

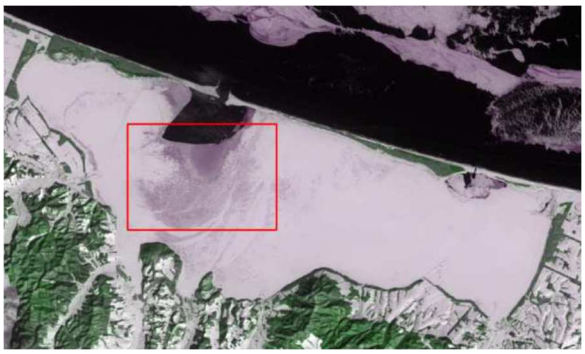

(a) RSI image

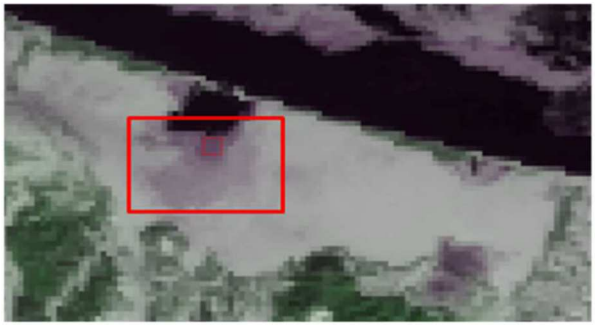

(b) MODIS image

Figure 9. Comparison of RAI image with MODIS image (Saroma Lake, February 19, 2011)

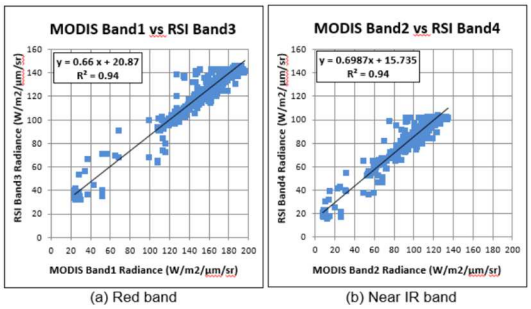

(a) Red band (b) Near IR band

Figure 10. Scatter plots of RSI radiance vs MODIS radiance. (Saroma Lake, February 19, 2011)

4.4 Thin Ice Area Extraction Algorithm

The authors have been developing the thin ice area extraction algorithm using MODIS data for the past several years (Hayashi et al., 2017). After some modification, the following is the concept of the latest algorithm. Figure 11 shows a color composite image of MODIS assigning blue & red to band 1(visible) and green to band 2(near IR). In order to investigate the possibility of extracting thin ice area using MODIS data, the authors have selected the test areas for thin ice, open water, cloud, and big ice floe from the MODIS image of the Sea of Okhotsk observed on February 26, 2021 as shown on Figure 11. Figure 12 show the scatter plot of the four test areas of big ice floe(■), thin ice(▲), cloud(◆), and open water(●) plotted on the Band1 VS Band2 diagram. The gray dots(■) correspond to the whole distribution of the data in the Sea of Okhotsk. Considering the distribution of each item in Figure 12, the authors have derived the following two equations to extract the thin ice areas.

$$B2<0.60\times B1+3 \quad (1)$$
$$2<B1<35 \quad (2)$$

Where B1: Reflectance of MODIS Band 1
B2: Reflectance of MODIS Band 2

By using the equation (1) and (2), the pixels which are plotted in the red meshed area in Figure 12 will be classified to thin ice area in this algorithm. Figure 13(b) show the thin ice area extracted result overlaid on the MODIS image. It is clear that Most of the dark purple areas shown on the MODIS image are well extracted.

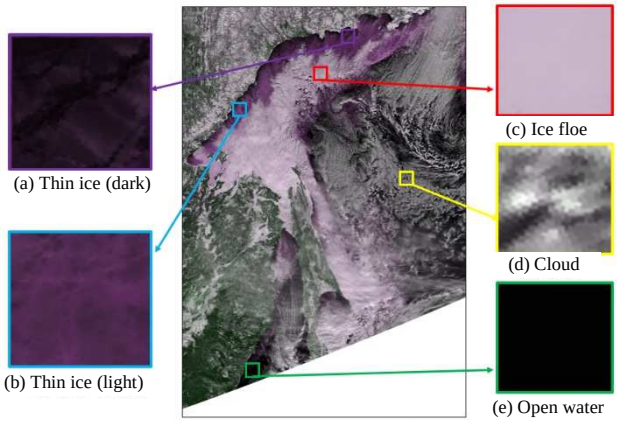

Figure 11. Extraction of test area from the MODIS image.
(Sea of Okhotsk, February 26, 2021)

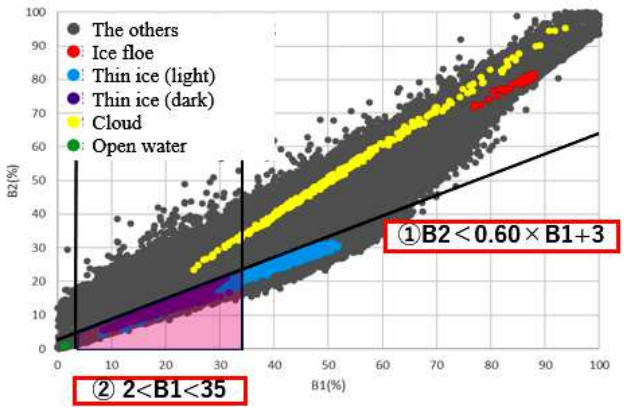

Figure 12. Concept of thin ice area extraction using the scatter plot of MODIS Band 1 vs Band 2.
(Sea of Okhotsk, February 23, 2014)

In this algorithm, the key points are parameter setting of equation (2). Originally the authors were using 5<B1<55 for extracting thin ice areas. However, after evaluating many MODIS images, it has become clear that some of the thin ice areas were rejected as open water. Finally, the lower limit threshold was changed from 5 to 2. In same manner, the upper limit threshold was changed from 55 to 35 to reject brighter ice areas. Setting upper limit threshold of thin ice to 35% is quite reasonable considering the ice reflectance measurements (See Figure 5 and 6). Also, since the MODIS data is the average reflectance of 250m x 250m area, the reflectance of ice area may become lower in MODIS data than the reflectance of pure ice.

On the other hand, the dark areas in the MODIS image of Figure 13 look like open water. It is difficult to evaluate if they are open water or dark thin ice by only looking at the MODIS image. Also, the light purple areas look like thin ice areas. So, authors have decided to collect MODIS and Landsat OLI images observed on the same day and use OLI images for validation. The authors have applied this algorithm to several scenes of MODIS and compared them with Landsat OLI images observed on the same day in the Sea of Okhotsk.

(a) MODIS image

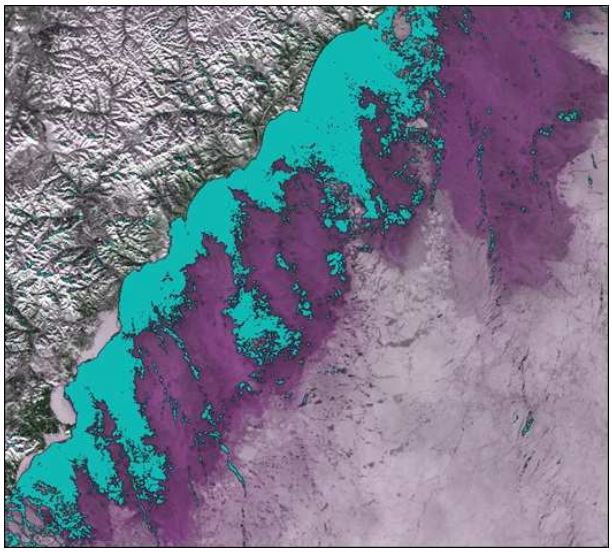

(b) Extracted thin ice areas overlaid on the MODIS image.

Figure 13. Thin ice area extracted result.

This contribution has been peer-reviewed. The double-blind peer-review was conducted on the basis of the full paper.
https://doi.org/10.5194/isprs-annals-V-3-2022-319-2022 | © Author(s) 2022. CC BY 4.0 License.

5. EVALUATION OF EXTRACTED RESULT

Total of three cloud free OLI images including thin ice areas were selected in the Sea of Okhotsk as shown on Figure 14 for the algorithm validation. The MODIS images of the same areas observed on the same days were processed and thin ice areas were extracted. In this section, the MODIS color composite is Band1: blue & red, Band 2: green, and the OLI color composite is Band 4: blue & red, Band 5:green. The thin ice areas extracted from MODIS are overlaid on each MODIS image.

Figure 14. Test sites of the validation.

(a) Site-A

Figure 15(a) shows the extracted thin ice areas overlaid on the MODIS image of Site-A observed on February 16, 2021, and Figure 15(b) shows the OLI of the same area observed on the same day.

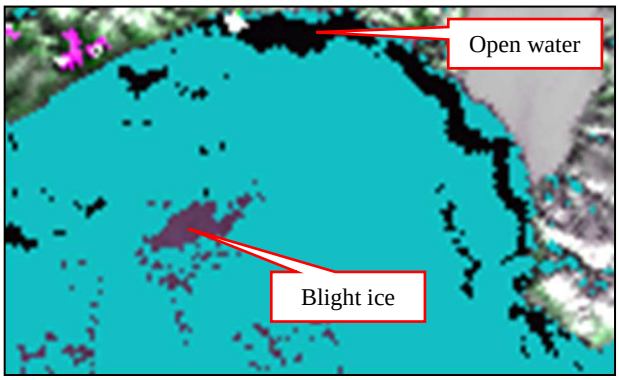

(a) Extracted thin ice area overlaid on MODIS image.

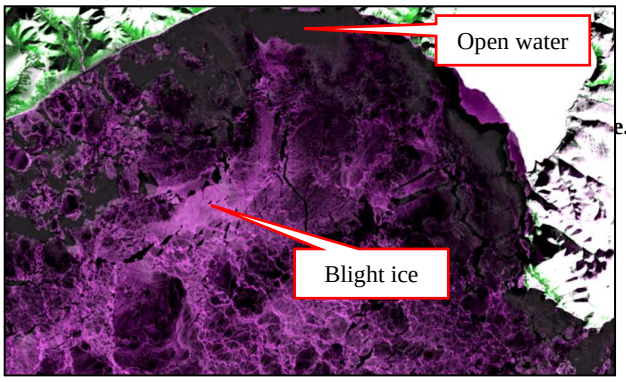

(b) OLI image of the same area

Figure 15. Comparison of MODIS and OLI images of Site-A. (February 16, 2021, Sea of Okhotsk)

Most of the thin ice area appearing in dark purple in the OLI image were well extracted with this algorithm. At the same time, the open water along the coast of Russia and bright ice area in the center of the OLI image are well rejected from thin ice areas. On the other hand, some of the areas which look like open water along the coast of Russia were extracted as thin ice areas. This suggests the importance of tuning the threshold of equation for open water rejection.

(b) Site-B

Figure 16(a) shows the extracted thin ice areas overlaid on the MODIS image of Site-B observed on March 7, 2021, and Figure 16(b) shows the OLI of the same area observed on the same day. Most of the thin ice areas appearing in dark purple in center of the OLI image were well extracted with this algorithm. At the same time, the open water along the coast of Russia and bright ice area in the right-hand side of the OLI image were well rejected from thin ice areas. However, the tuning of the threshold of equation (2) for rejecting thicker ice based on the in-situ measurement is necessary for improving the algorithm.

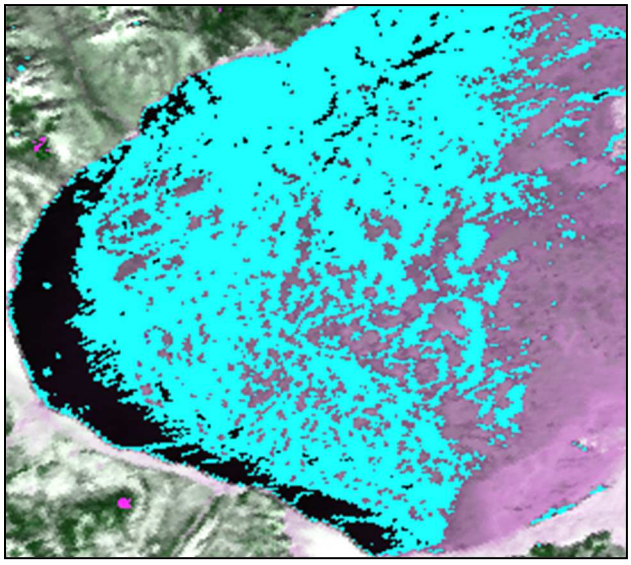

(a) Extracted thin ice area overlaid on MODIS image.

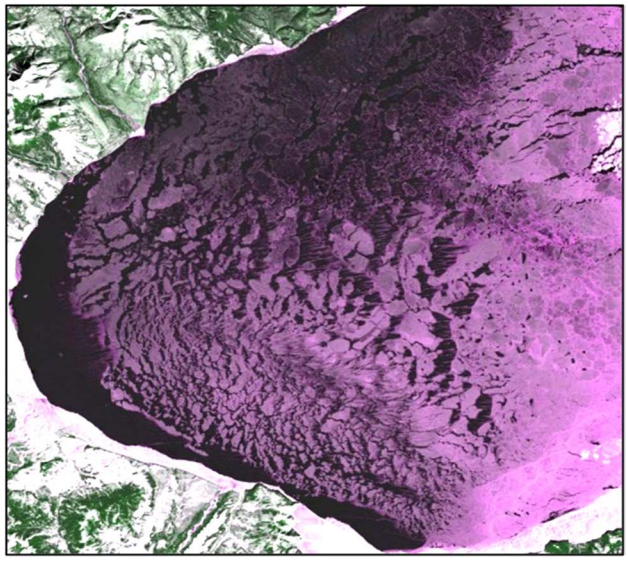

(b) OLI image of the same area.

Figure 16. Comparison of MODIS and OLI images of Site-B. (March 7, 2021, Sea of Okhotsk)

This contribution has been peer-reviewed. The double-blind peer-review was conducted on the basis of the full paper.
https://doi.org/10.5194/isprs-annals-V-3-2022-319-2022 | © Author(s) 2022. CC BY 4.0 License.

(c) Site-C

Figure 17(a) shows the extracted thin ice areas overlaid on the MODIS image of Site-A observed on February 16, 2021, and Figure 17(b) shows the OLI of the same area observed on the same day. Most of the thin ice areas in the upper part of Gulf of Patience of the Sakhalin appearing in dark purple in the OLI image were well extracted with this algorithm.

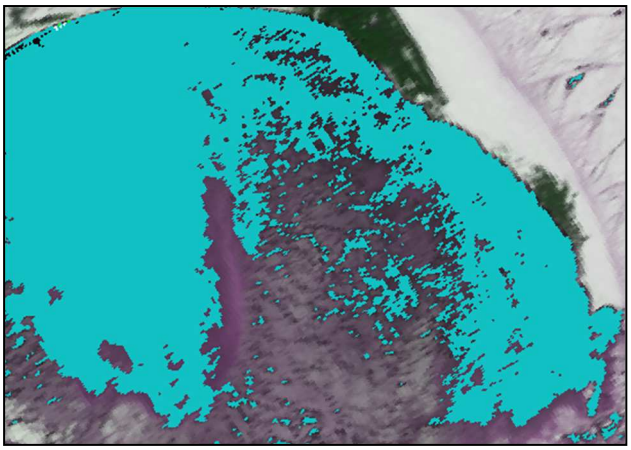

(a) Extracted thin ice area overlaid on MODIS image.

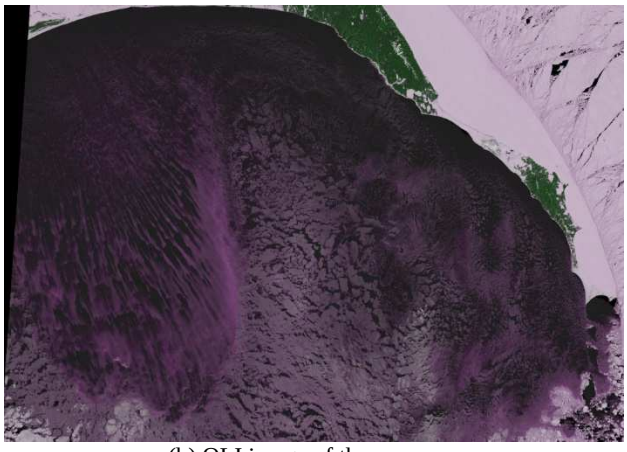

(b) OLI image of the same area.

Figure 17. Comparison of MODIS and OLI images of Site-C. (February 27, 2021, Sea of Okhotsk)

6. CONCLUSION

In this study, the authors have examined the possibility of extracting thin ice areas from optical sensor data. Since the reflectance of sea ice is likely to be affected by the freezing condition and snow cover, the estimation of ice thickness using optical sensors is not easy. Also, the reflectance of ice would be saturated at certain thickness and snow cover. However, through the comparison of in-situ measurement with satellite observation, the possibility of extracting thin ice areas from optical sensor data was suggested. Based on these experiences, the authors have developed a method to extract thin sea ice areas using the scatter plots of reflectance derived from MODIS Band 1 and 2 data. By applying the two equations to the MODIS Band 1&2 domain, most of the thin ice areas which were visually recognized in the MODIS images were well extracted not only in the Sea of Okhotsk. The comparison of the extracted results with high resolution OLI images of Landsat 8 suggested the reliability of the method. Some of the thin ice area extracted with this algorithm were recognized as open water in the MODIS image. However, most of them were recognized as thin ice areas in the OLI images.

The key point of this algorithm is the parameter setting of equation (2). Talking about the lower limit threshold, 3 is reasonable in most cases. However, sometimes 2 or 4 is better. As for the upper limit threshold, the authors have chosen 35 so far. However, the tuning of the upper limit threshold for rejecting thicker ice based on the in-situ measurement is necessary for improving the algorithm. The authors are testing the algorithm to the other seasonal sea ice zone of the northern hemisphere including the Bering Sea and in the Gulf of Saint Lawrence. The initial result is quite promising, and the detailed study will be followed. Our next step is to identify the highest thickness which can be extracted as thin ice areas with this algorithm.

ACKNOWLEDGEMENT

This study was supported by JAXA under the framework of GCOM-W Verification Program. The FORMOSAT-2 data were provided from NSPO and NCU. The authors would like to thank JAXA, NSPO, and NCU for their kind support. The authors also would like to thank the graduated students at Tokai University namely Yusuke Mochizuki, Atsushi Komaki, Kazuya Hayashi and Rio Kanisawa for their great contribution to this study.

REFERENCES

IPCC, 2021, “Summary for Policymakers.” in Climate Change 2021: The Physical Science Basis, Contribution of Working Group I to the Fifth Assessment Report.

Allison, I., 1993, East Antarctic sea ice: albedo, thickness distribution, and snow cover”, J. Geophys. Res., Vol. 98, pp.12417-12429.

Perovich , D. K. and T. C. Grenfell, 1982, A theoretical model of radiative transfer in young sea ice, J. Glaciol., Vol.28, pp. 341-356.

Grenfell, T. C., 1983, A theoretical model of the optical properties of sea ice in the visible and near infrared, J. Geophys. Res., 88, 9723-9735.

Mäkynen, M., J. Karvonen, 2017, MODIS Sea Ice Thickness and Open Water–Sea Ice Charts over the Barents and Kara Seas for Development and Validation of Sea Ice Products from Microwave Sensor Data, Remote Sensing 9, no. 12, 1324.

Maykut, G. A., 1978, Energy exchange over young sea ice in the central arctic, JGR, Vol.83, pp.3646-3658.

ASD FieldSpec HandHeld, 2006, http://www.asdi.com/products-fshh-fshhp.asp

Cho, K., Y. Mochizuki, Y. Yoshida, M. Nakayama, K. Naoki, C.F. CHEN, 2011, Thin ice thickness monitoring with FORMOSAT-2 RSI data, Proceedings of the 32nd Asian Conference on Remote Sensing, TS1-2, pp.1-8.

Cho, K., Y. Mochizuki, Y. Yoshida, H. Shimoda and C.F. CHEN, 2012, A study on extracting thin sea ice area from space, International Archives of the Photogrammetry, Remote Sensing and Spatial Information Sciences, Vol. XXXIX-B8, pp.561-566.

Hayashi, K., K. Naoki, K. Cho, 2017, Extraction of thin ice area using MODIS data in the seasonal sea ice zones of the northern hemisphere, Proceedings of the 38th Asian Conference on Remote Sensing, ID:764, pp.1-5.

NASA, 2017, MYD09, https://ladsweb.modaps.eosdis.nasa.gov/api/v1/productPage/product=MYD09

NASA, 2010, http://modis.gsfc.nasa.gov/

USGS, 2014, https://landsat.usgs.gov/landsat-8-l8-data-userhandbook